Open Research Online

The Open University's repository of research publications
and other research outputs

A new approach to estimating hazard posed by debris flows in the Westfjords of Iceland

Journal Item

For guidance on citations see FAQs.

oro.open.ac.uk

Accepted Manuscript

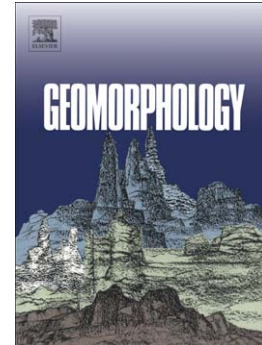A new approach to estimating hazard posed by debris flows in the Westfjords of Iceland

S.J. Conway, A. Decaulne, M.R. Balme, J.B. Murray, M.C. Towner

Please cite this article as: Conway, S.J., Decaulne, A., Balme, M.R., Murray, J.B., Towner, M.C., A new approach to estimating hazard posed by debris flows in the Westfjords of Iceland, *Geomorphology* (2009), doi: 10.1016/j.geomorph.2009.08.015

A new Approach to Estimating Hazard posed by Debris Flows in the Westfjords of

Iceland

S.J. Conway[a]*, A. Decaulne[b], M.R. Balme[a], J.B. Murray[a] and M.C. Towner[c]

[a]*Department of Earth and Environmental Sciences, Open University, Milton Keynes MK7 6AA, UK*

[b]*University Blaise Pascal, CNRS UMR6042 Geolab, Clermont-Ferrand, France*

[c]*Impacts and Astromaterials Research Centre, Department of Earth Science and Engineering, Imperial College London, SW7 2AZ, UK*

*Corresponding author. Tel.: +44 (0)1908 659777; Fax: +44 (0)1908 655151; E-mail: s.j.conway@open.ac.uk.

1 A new Approach to Estimating Hazard posed by Debris Flows in the
2 Westfjords of Iceland

3 Conway, S. J.[a] (corresponding author), Decaulne, A.[b], Balme, M. R. [a], Murray, J. B.[a] and

4 Towner, M. C. [c]

5 [a] Department of Earth and Environmental Sciences, Open University, Milton Keynes

6 MK7 6AA, UK. s.j.conway@open.ac.uk tel:+44 (0)1908 659777 fax:+44 (0)1908 655151

7 [b]University Blaise Pascal, CNRS UMR6042 Geolab, Clermont-Ferrand, France.

8 [c]Impacts and Astromaterials Research Centre, Department of Earth Science and

9 Engineering, Imperial College London, SW7 2AZ, UK.

10 **Abstract**

11   The aim of this study is to improve the assessment of hazard posed by debris flows to

12 the people and settlements of northwest Iceland by studying very recent examples from above

13 the town of Ísafjörður and other nearby localities. Debris flows are a recognised hazard in the

14 region: above Ísafjörður, they occur with particularly high frequency and have appreciable

15 volumes (up to 14 000 m^3). We have used airborne laser altimeter (LiDAR) and differential

16 Global Positioning System (GPS) data to produce isopach maps of flows that occurred in

17 1999, 2007, and 2008. Our data show that these flows begin depositing at higher slope

18 gradients and are also more mobile than hillslope debris flows reported by other authors.

19 Above a 19° slope, erosion is initiated independent of the distance along the flowpath. Using

20 the isopach maps and associated field observations, we have found a relationship between

21 ground slope and patterns in deposition volume. We have used this finding as a basis for an

22 empirical model that enables an estimate of the total travel distance and final thickness of

23 future debris flows to be calculated. This has enabled us to identify areas of the town which

24 are at risk; some of these are not obvious without this analysis. This model is notable for its

25 simplicity, which allows future debris flow characteristics to be predicted without the need to

26   determine the precise fluid dynamic parameters of the flow such as viscosity and velocity,

27   which are required to implement more complex models.

28

29   *Keywords:* debris flow; Icelandic Westfjords; geohazards; LiDAR

30   1. Introduction

31   *1.1. Background*

32   Debris flows move at great speed (e.g., 0.8-28 ms^{-1} from debris flows measured in the

33   field; Rickenmann, 1999) and are able to carry metre-size boulders (e.g., Clague et al., 1985;

34   Kanji et al., 2008). They have great destructive ability and can pose a significant hazard to

35   people and infrastructure. We have begun a new study in the Westfjords region, situated in

36   the north-western tip of Iceland (Fig. 1), where the infrastructure and local population are at

37   considerable risk from a variety of slope-process hazards, including avalanches, landslides,

38   slush-flows, rock falls, and debris flows. Many recent incidents related to snow avalanches

39   have been serious: for example, 20 people died in a single avalanche in Flateyri in 1995

40   (Arnalds et al., 2004). These events have stimulated study of these processes in this region,

41   and as a result government agencies have defined hazard zones (Arnalds et al., 2002). Debris

42   flows have not caused major loss of life in this area in recorded history (Decaulne et al.,

43   2005), but with the expansion of the traditional settlements from spits in the middle of the

44   fjords toward the hillslope, it becomes increasingly likely that a debris flow event will occur

45   that results in considerable destruction or death. Residents report the frequent blocking of

46   roads by debris flows, and in 1999 several flows overcame the lower slope ditch (marked in

47   Fig. 2), which was built to protect the town and damaged houses in Ísafjörður (Decaulne et

48   al., 2005). The main purpose of this study is to reassess the hazard posed to these new

49   settlements using improved data on recent debris flows.

50

51   **[Fig. 1 here]**

52

53   The focus of debris flow hazard prediction models is skewed toward so-called confined

54   debris flows, which travel along confined preexisting channels or torrents and emerge on to

55   alluvial or debris fans (Rickenmann, 1999; Berti and Simoni, 2007; Gartner et al., 2008;

56   Prochaska et al., 2008). In contrast, few studies concentrate on the hazard posed by hillslope-

57   style debris flows (Fannin and Wise, 2001), which are not restricted by preexisting valleys

58   over the majority of their length. Hillslope debris flows are common in steep terrain

59   throughout the world; however, these types of flows form significant recognised hazards in

60   Iceland (Decaulne and Sæmundsson, 2007) and Scandinavia (Rapp and Stromquist, 1976).

61   This study presents new results from quantification of the volume and pattern of debris

62   flow deposits using topography digital elevation models (DEMs) generated from differential

63   GPS (global positioning system) measurements, and from LiDAR (light detection and

64   ranging) data. This aim of this study is to improve hazard assessment in the region by

65   empirical description of hillslope debris flows.

66   *1.2. Regional setting*

67   Our study area in the Westfjords area of Iceland (Fig. 1) is a typical post-glacial

68   landscape consisting of deep fjords cut into a sequence of basaltic lava flows of Miocene age

69   (~ 15 Ma). The hillsides in the Westfjords area rise from sea level to 700 m with average

70   slope angles of 25-35°. The slopes are rocky and poorly vegetated; the dominant species are

71   grasses and mosses on the soils and lichens on the rocks. The fjords themselves are incised

72   into 2-30 m thick layers of basalt rock, which dip gently toward the SE (Decaulne et al.,

73   2005). The slopes are very steep in the upper portion (~ 45°) and often form bedrock cliffs.

74   The lower slopes comprise talus and relict debris flow deposits. The channels that dissect

75   these slopes are principally incised by debris flows. These channels can lie as close together

76   as 15 m, are densely packed along most of the slopes in the study area, and often span the

77   entire slope from top to bottom (up to 1.5 km in places). The area retains many inherited

78   glacial features as well as active paraglacial features that include solifluction lobes and thick

79   surface deposits of till on flat surfaces. Active slope processes are common here, most

80   probably as a result of the post-glacial slope readjustment that has been ongoing over the last

81   10 ka since glacial retreat (Norðdalh, 1990). The temperatures in the area usually vary

82   between -5 and 10°C with the 30 year mean annual precipitation being ~2000mm/yr. Much

83   of the precipitation falls as snow and snow patches can be preserved in shadow into the

84   summer months. The maritime position of the Westfjords means that snow cover can be very

85   variable and liable to thaw suddenly even in winter.

86

87   **[Fig. 2 here]**

88

89   The town of Ísafjörður is mostly located on a spit formed by the action of the sea, with

90   expansion of the town over the last 50 years being accommodated along the basal slopes of

91   the fjord. The slope above Ísafjörður (Fig. 2C) is interrupted at ~ 450 m altitude by the

92   Gleiðarhjalli bench, which slopes gently to the SE and is covered by ~ 30 m of glacial

93   sediments; these comprise gravelly to silty sand and subangular to subrounded clasts that

94   range in size from centimetre to metre. On top of these deposits lie many centimetres to

95   metres sized angular clasts derived from frost shattering of the bedrock and glacial clasts

96   themselves. These sediments reach the angle of repose very quickly, as frost shattering

97   promotes erosion of the bedrock cliff at their base and creep pushes the sediment body

98   forward toward the bench edge. This means that the debris flows above Ísafjörður are not

99   supply limited, but limited by the frequency of triggering events, unlike most other flows in

100   the area (Glade, 2005).

101   Debris flows in this area are triggered by rapid snowmelt or prolonged rainfall (Decaulne

102   et al., 2005; Decaulne and Sæmundsson, 2007). These processes saturate the sediment stack,

103 which further destabilises the already unstable sediments. A debris flow is then triggered as a

104 result of undercutting of these sediments by water emerging from beneath the sediment stack

105 at the interface with the basalt bedrock. Rockfalls originating at the exposed edge of the

106 debris stack have been observed immediately prior to a debris flow and are a probable cause

107 of failure (Decaulne et al., 2005). The glacial till fails by rotational sliding and then forms a

108 debris flow.

109   The mean interval between large flows is only five years (Decaulne et al., 2005). On

110 other slopes in Iceland, debris flows are much less frequent and generally smaller because

111 they are supply limited (Glade, 2005) — the debris on the slopes must reach a certain

112 thickness and steepness before it can slide (Ballantyne and Benn, 1994; Wilkerson and

113 Schmid, 2008). The debris flows above the town of Ísafjörður provide a unique opportunity

114 to study debris flows because (i) the frequency of large events is unusually high and (ii) the

115 majority of the deposits are preserved on the slopes. This means that we have the opportunity

116 to study very fresh debris flows in which the influence of post-depositional reworking is

117 minimised, thus allowing more accurate quantification of erosion and deposition volumes and

118 patterns.

119   In addition to the SE-facing slope above Ísafjörður, two additional sites (Figs. 2A and

120 2B) were selected because they had also experienced fresh debris flows just prior to the field

121 visits in 2007 and 2008. Firstly, we studied an area to the south of Hnífsdalur, a village

122 located to the north of Ísafjörður. Debris flows are much less frequent here than in Ísafjörður,

123 but we investigated a small fresh flow sourced from the soil mantle on the slope above the

124 valley road, which occurred here in late spring or early summer 2007. This flow originated, in

125 all likelihood, as a failure triggered by concentration of overland flow that then eroded

126 downslope before deposition. Secondly, on the north side of Súgandafjörður, debris flows

127 regularly block the road and two fresh flows had cut off the road between Botn and Grensfjall

128   between the 2007 and 2008 field visits. The flows originate by the "fire hose" (e.g., Johnson

129   and Rodine, 1984; Coe et al., 2007; Carrara et al., 2008) mechanism in alcoves cut into the

130   bedrock cliffs bounding the fjord. This triggering mechanism is characterised by the

131   concentration of overland flow by chutes or depressions in the bedrock that evolves into a

132   debris flow as it picks up material from the slope where it emerges. This material has to build

133   up by weathering and erosion of the bedrock before a debris flow can be formed (as for

134   Glade, 2005), hence the time between large events is much longer than at Ísafjörður. The

135   source material is the product of frost shattering of material that has collected in these alcoves

136   under the action of gravity. Interestingly, the flows did not originate from the top of the fjord

137   (700 m asl) but from material accumulated at ~ 500 m or lower.

138

139   **2. Materials and methods**

140   *2.1. Previous work and methodology for this study*

141   Debris flow volumes are usually estimated from either the failure scar (e.g. Gabet and

142   Bookter, 2008) or the deposits themselves (e.g. Decaulne et al., 2005). Traditionally this is

143   done by measuring cross sections and long sections of the features, although the precise

144   method and associated errors are rarely reported (e.g., Rapp and Nyberg, 1981; Gardner,

145   1989; Okuda, 1989; Decaulne et al., 2005). Exceptions to this include Santi et al. (2008), who

146   report errors as small as ± 23 % on volume estimation using the cross section technique with

147   a slope profiler. They take into account the variation in technique between individuals and the

148   use of differing locations for the cross sections, but do not include an error associated with

149   estimating the pre-flow topography. A report that examined methods for estimating the

150   erosion volumes removed by rills (Casali et al., 2006) recommended that sampling by

151   microtopographic profile meter, which produces 50 points over 1 m to get an error of < 10%

152   in volume calculation.

153   Empirical estimates of volumes have been derived from morphological data (e.g.,

154   Larsson, 1982; Innes, 1983; Fannin and Wise, 2001), but these rely on a large sample size

155   and their applicability varies by region. Empirical relationships from large data sets relating

156   volumes, total travel distance, and other dimensions have been found for confined debris

157   flows (Rickenmann, 1999) and hillslope debris flows (Lorente et al., 2003), but neither of

158   these empirical approaches give information on the structure and pattern of deposition and

159   erosion. Iverson, et al. (1998) produced a widely applied model called LAHARZ, which

160   calculates the inundation of a debris flow given a DEM. This routine produces a set of

161   potential debris flow inundation zones with an associated hazard rating based on their

162   statistical analysis. It is based on empirical equations relating cross sectional area and

163   inundation area to total volume. However, this analysis is not reliable if the flows are

164   unconfined over most of their length, as the equations are derived from the study of 27

165   confined lahars originating from nine volcanoes. It does not attempt to estimate eroded

166   volumes or deposition volumes along the flow. Fannin and Wise (2001) produced an

167   empirical–statistical model that calculates erosion and deposition per reach of the flow, with

168   the equations dependent on whether the flow is confined, transitional, or unconfined. It is

169   based on the study of 449 debris flow events in Queen Charlotte Islands, British Columbia,

170   Canada. This model comes closer than other empirical models to describing the realistic

171   behaviour of debris flows without full flow dynamic modelling.

172   Repeat stereo photogrammetry has been used to estimate overall slope denudation (Coe

173   et al., 1997; Breien et al., 2008). Coe et al. (1997) used a 2 x 2 m grid and achieved a volume

174   error of ±5%. Breien et al. (2008) used a 3.3 x 3.3 m grid and achieved an error of ±10%.

175   Neither study revealed the fine-scale structure of the debris flows (e.g., the levees were

176   poorly resolved). In landslide studies LiDAR is often used in conjunction with other datasets,

177   e.g., Chen et al. (2006) used DEMs derived from photogrammetry to compare with LiDAR

178 topography. However, the lower accuracy of the photogrammetry and the difficulty in

179 georeferencing all the datasets meant that the authors were only able to detect 10-100 m

180 vertical changes. Good results have been obtained by comparing repeated LiDAR surveys

181 (Scheidl et al., 2008) with estimated errors in the volume calculation ranging from just 9% up

182 to 55%. No repeat LiDAR surveys have been performed in the Westfjords area, so we have

183 used a combination of LiDAR data and differential GPS data to quantify the changes in

184 morphology along the debris flows.

185 *2.2. Data collection*

186 Eight debris flows were surveyed using a Leica System 500 differential GPS (Fig. 2) in

187 2007-2008. Five debris flows were examined on the slopes above Ísafjörður (Fig. 2C): one on

188 the slope above Hnífsdalur in the adjacent valley (Fig. 2B), and two on the east slopes of

189 Súgandafjörður (Fig. 2A). The relative timing of the activity of the debris flows in this study

190 is shown in Table 1. A base GPS unit was positioned at the foot of the slope within 3 km of

191 the rover GPS units. Point elevation data were collected by two roving units, with the

192 operator collecting three or more epochs of data per point. To ensure high quality, data were

193 not collected when the Global Dilution of Precision (GDOP) value (which is calculated real-

194 time from relative satellite positions) was > 7. A Leica System 800 Total Station (TPS) was

195 used to collect additional data in 2008. The location and orientation of the TPS was obtained

196 by collecting shared points with the GPS. The TPS collects point elevation data using a laser

197 ranger equipped with accurate internal determinations of horizontal and vertical angles. The

198 TPS could collect points at a maximum distance of 450 m.

199 Four main types of sampling were performed:

200 (i) channel long profile: recording the lowest point between the levees;

201 (ii) levee long profile: recording the maximum elevation of the levees on each side of the

202   channel;

203   (iii) cross profiles: taken at ~ 50 m intervals (10 m for 5DF, 20 m for 7,8,10DF) along the

204   debris flow; and

205   (iv) debris flow edge: only measured if the flow was well defined.

206 For each of these methods the topography was sampled at 0.5-2.0 m intervals, with more

207 frequent sampling used where the topography changed more rapidly. This frequency of cross

208 sections follows the scaled-up methodology advised by Casali et al. (2006).

209   The GPS data were supplemented with LiDAR data acquired using an Optech

210 ALTM3033 instrument and aerial photography taken with a Leica-Wild RC10. These data

211 were collected on 5 August 2007 by the U.K. Natural Environment Research Council's

212 Airborne Research and Survey Facility (NERC ARSF; Fig. 1). Seventeen flight lines were

213 flown allowing the collection of 63 million LiDAR points and 63 aerial photographs. The

214 aerial photographs were orthorectified, mosaiced, and georeferenced using BAE System's

215 SocetSet software.

216   Further processing of the LiDAR data was required to correct for between-track

217 horizontal shifts of up to 2 m, which in steep areas results in an equivalent magnitude of

218 vertical error. This problem has been highlighted by Favalli et al. (2009) and they state that

219 sub-metre scale measurements cannot be taken without correction for these between-track

220 errors. To achieve this correction we used a least squares matching technique developed by

221 Akca (2007a, b), which matches the surface shape and LiDAR intensity between each track

222 to align the tracks relative to one another. This adjusted data set was then georeferenced by

223 aligning it to the GPS data collected in the 2007 campaign. This processing resulted in the

224 cross-track and georeferencing errors in the LiDAR data being reduced to ~0.1 m vertically

225 and < 0.25 m horizontally as detailed in Table 2.

226 *2.3. Generation of elevation models*

227   To measure volumes of debris flows, we calculated the slope shapes before and after

228 debris flows. In all calculations we used the last return LiDAR data where the height of the

229   ground at the LiDAR shot point is calculated using the return time of the last laser light to

230   reach the receiver from that particular shot. We used these data to create a regional 5-m DEM

231   using the LiDAR Explorer 2.0 extension for ArcGIS. This program uses the mean value of

232   the LiDAR shots within each pixel to produce a smooth DEM and if necessary uses linear

233   interpolation between the LiDAR shots to fill small data gaps.

234   The combined 2007 GPS and last return LiDAR survey data for the debris flows were

235   converted into local 0.25-m DEMs for each debris flow. This was performed using the

236   universal Krige interpolation method provided within the geostatistical analyst tool of ESRI's

237   ArcMap software, which has been verified as a valid method for this type of data (Scheidl et

238   al., 2008). We used Krige rather than Natural Neighbour, as recommended by Scheidl et al.

239   (2008), because the Krige method allows inclusion of the expected asymmetry of the surface

240   as well as the asymmetry of the sampling, and provides an estimation of the errors associated

241   with the prediction. Because of the relatively low number of points compared to those

242   processed by Scheidl et al. (2008), this processing was computationally inexpensive to

243   perform — high cost being the main argument presented against this method by Scheidl et al.

244   (2008).

245   For those debris flows that occurred before the LiDAR survey (1DF, 2DF, 3DF, and

246   5DF), the pre-flow morphology was estimated using the 2007 data alone. This was achieved

247   by taking all the GPS and LiDAR points within a 5-m buffer around the boundary of the flow

248   (i.e., excluding all the points that lie on the new debris flow) and performing a Krige

249   interpolation based only on these points — in essence "smoothing out" the debris flow to

250   estimate the preexisting topography. Where the debris flow is wide, especially in the alcoves,

251   the interpolation was performed across large distances (of the order of 50 m). The post-flow

252   surface was estimated using all of the 2007 data across the flow. For those debris flows which

253   occurred after the LiDAR survey (7DF, 8DF, and 10DF), the pre-flow morphology was

254   interpolated from the 2007 LiDAR and GPS data and the post-flow morphology derived from

255   the 2008 GPS and TPS data.

256   *2.4. Volume estimation and patterns*

257   To assess trends in deposited volume over the length of the debris flow, the GPS points

258   representing the margins of the debris flow were converted into a polygon shapefile using

259   ArcGIS software. This polygon was then split into along-flow segments (Fig. 3). These

260   segments were equally spaced and lay perpendicular to the channel centre line (i.e., they were

261   not necessarily of equal area). Section length was at 5-m intervals for all debris flows —

262   apart from the small debris flow, 5DF, which had a 2-m interval. For each debris flow, an

263   isopach map was produced by subtracting the post-flow surface from the pre-flow surface.

264   Then for each segment, the total volume of erosion and of deposition was calculated by

265   summing the negative and positive pixels, respectively, of the isopach map falling within the

266   segment. To account for the varying areas of each segment, the volumes were divided by the

267   area of the segment, giving a representative thickness (of erosion and deposition) for each

268   segment. The concept of representative thickness is a proxy for volume.

269

270   **[Fig. 3 here]**

271

272   The segmented polygons were then used to generate statistics based on underlying

273   topography. To analyse how the flow responded to variations in the regional slope

274   morphology, we used a 5-m DEM produced from the LiDAR data. To analyse responses to

275   the morphology produced by the flow itself, we used the higher resolution 0.25-m DEMs

276   produced for each debris flow from LiDAR and GPS data. For each DEM, the mean slope

277   angle and elevation were calculated using the standard tools provided in Spatial Analyst of

278   ArcGIS. The slope angle is derived using the steepest downhill slope as calculated by fitting a

279   plane through the eight nearest neighbours.

280   To analyse patterns of erosion and deposition in all the flows together we normalised

281   their individual segment erosion and deposition representative thicknesses. Normalisation is

282   performed for erosion and deposition separately and is calculated by dividing representative

283   thickness for each segment by the total representative thickness for each flow (of erosion or

284   deposition as appropriate) so that data for all the flows can be compiled together (otherwise

285   the signal from the largest, freshest debris flow would dominate). This normalisation then

286   adjusts for differences in both scale and age.

287

3. Results

288

289   *3.1. Field observations – sources of materials and changes over time*

290   All the debris flows in this study form levees, and some exhibit a terminal lobe. The

291   levees flank the channel and, when large and fresh, have steep interior and exterior slopes.

292   The levees all contain a fine matrix that supports the clastic material; however, the source

293   material and age of the deposits varies between flows.

294   Decaulne (2001) observed that debris flows 2DF, 3DF, and 4DF were sourced from a

295   rotational slide of the glacial material on top of Gleiðarhjalli bench. This material is

296   characterised by the high content of subrounded to subangular clasts ranging from

297   centimetres to metres in size supported by 10-30% orange-brown fines (see grain-size

298   analysis in Decaulne et al., 2005). We found that the materials that compose the levees in

299   debris flow 1DF matched the glacial deposits. Hence, the composition of the levees reflects

300   the composition of the source area. We used visual inspection and correlation to determine

301   the source deposits of the remaining flows in this study (Table 3). The precise drainage areas

302   for the Ísafjörður debris flows (1DF, 2DF, 3DF, 4DF, and 7DF) are hard to determine as

303   much of the water flow occurs beneath the surface of the bouldery Gleiðarhjalli bench. Most

304   of the contributing area is from the Gleiðarhjalli bench, with some contribution coming from

305   the small plateau on the slope above. The other debris flows (5DF, 8DF, and 10DF) have

306 rockwall chutes upstream, which have small (or negligible in the case of debris flow 5DF)

307 plateaus above them.

308   We have observed that debris flows usually take the path of a previous flow for at least

309 the upper third of the total length. Levees that have been washed free of fines can be

310 infiltrated by them again in a subsequent flow and in addition the levees can be built up in

311 height. When flows are frequent, this means that caution is required when estimating the

312 volume without knowledge of preexisting topography. Other authors have noted that levees

313 are often reworked in subsequent flows, leaving almost no evidence of the previous flow,

314 which leads to underestimation of historical frequency (e.g., Luckman, 1992).

315   Decaulne (2001) reported anthropomorphic removal of material from debris flows 2DF

316 and 3DF because they affected the town. At debris flow 7DF, we observed that a significant

317 quantity of material had been mechanically excavated from the ditch to the bank between the

318 2007 and 2008 field visits. These deposits were therefore not included in our study, and this

319 anthropomorphic modification should be considered when drawing conclusions from volume

320 data. We observed that large quantities of material had been moved from the road to the

321 downslope verge in debris flows 8DF and 10DF, however, these deposits were included in

322 our survey. As the deposits were moved by 5 m or less, which is on the same order as our

323 sampling distance, we decided this was not sufficient to disrupt the conclusions based on the

324 analysis of volumes in this study.

325 *3.2. Debris flow volumes*

326   Table 4 presents estimates of volumes of the surveyed debris flows. According to the

327 classification of Innes (1983), these flows are medium-scale flows (except debris flows 5DF

328 and 7DF which are small-scale flows). On the 1-10 magnitude scale presented by Jakob

329 (2005) all the flows are rated as size class 2-3, with debris flow 5DF as size class 1-2.

330   To assess the performance of our method to estimate the pre-flow topography (see

331 section 2.3 for details) for debris flows 1DF, 2DF, 3DF, and 5DF, we also applied this

332 method to debris flows 7DF, 8DF, and 10DF, where the pre-flow topography is known from

333 the 2007 LiDAR survey. Table 4 shows the results of this analysis. Our method tends to

334 underestimate the overall volume of the flow by ~ 30-40 % and overestimate the erosion of

335 the flow by ~ 2-3 times. However, the overall volume of the erosion and deposition are not

336 important for the following analysis and hazard assessment, but the preservation of the

337 patterns of erosion and deposition. We find that the overall patterns of deposition and erosion

338 are preserved when using our method of estimating pre-flow topography for all the debris

339 flows (Fig. 4).

340

341 **[Fig. 4 here]**

342

343   The percentage errors appear large for all the flows (details of calculation in Appendix

344 A) for the following reasons:

345   (i) for those flows without pre-flow data, the interpolation (described in section 2.3) in

346 the lower surface was performed over long distances, resulting in large estimate errors,

347 especially in the source areas; and

348   (ii) because the error is expressed as a percentage, it is larger for the smaller debris

349 flows (5DF, 7DF, 8DF, and 10DF) as the absolute error forms a larger percentage of their

350 smaller volume. To put this in context, the average error on the deposition volume relates to a

351 ±20-cm thickness and the erosion volume corresponds to a ±42-cm thickness.

352   Despite the significant percentage errors that result from using the Krige interpolation

353 over large areas without points (see section 2.3 for details), it presents a superior approach

354 than just taking a linear surface under the flow. Firstly, because the method uses the

355 surrounding topography to estimate the pre-existing topography. Secondly, although the

356 linear and Krige interpolation methods perform equivalently (see Table 5), the Krige method

357   allows an estimate of potential error, whereas the linear method does not. In addition, we

358   compared our volume results to those obtained by extrapolation of the cross-sectional areas

359   calculated from cross profiles along the flow. We calculated the volume of debris flows 1DF

360   and 2DF using this method: once using all measured cross sections and again using just three

361   cross sections that are located at the same approximate position as those made by Decaulne et

362   al. (2005). Both methods produced equivalent estimates for volumes (Table 5), although we

363   must emphasise that when fewer cross sections are used greater care is required in ensuring

364   that they are representative of the flow as a whole (e.g., recommendations of Casali et al.,

365   2006). However, although extrapolation of cross-sectional area is adequate for estimating

366   volumes, it cannot be used for detailed study of the patterns of erosion and deposition.

367   *3.3. Patterns in erosion and deposition*

368   To demonstrate the overall patterns of erosion and deposition developed by debris flows,

369   we have chosen two case studies, debris flows 1DF and 5DF, to illustrate the behaviour. The

370   results from the calculation of total volumes of these debris flows are presented in Table 4,

371   and the spatial distribution of volume over the flow in Fig. 5. The scale of the two flows is

372   very different, but they both show slope-dependent behaviour. The relationship between

373   slope and the depositional regime is evident in Fig. 5, with slope directly affecting the pattern

374   and quantity of deposition as further detailed below.

375

376   **[Fig. 5 here]**

377

378   In debris flow 5DF (Fig. 5A), a transition between the erosion and depositional regimes

379   occurs at a sharp change of slope from 28° to 18°. The beginning of this slope change is

380   marked II on Fig. 5A.   Above this, the point at which levees begin to form is marked by a

381   slight decrease in slope, shown between I and II on Fig. 5A. A slight decrease in deposition

382   is matched by a slight increase in slope marked III, and a major peak in deposition occurs

383   about 50 m from the end of the flow, matched by a drop in slope at IV. For 5DF, the

384   complete cessation of erosion occurs somewhere between 25° and 17°, with deposition

385   starting at 32° (Fig. 5A). Field observations of *insitu* grass between the levees confirm that

386   erosion has stopped at this point. This flow remains mobile on slopes as low as 7°, but below

387   the lobe at IV field observations show the deposits have very little relief.

388   The main erosional section of 1DF (where deposition is negligible) terminates at a slope

389   angle of about 32° (marked I in Fig. 5B). Below this point, erosion continues to take place in

390   the centre of the channel, but temporarily ceases at the point where a secondary lobe breaks

391   off from the main flow and restarts below this, marked II. The main depositional phase is also

392   briefly interrupted over a short, steeper section (marked III) below which a brief pulse of

393   deposition occurs before the deposition tails off on to the lower slope section. The flow

394   remains mobile on slopes as low as 10°. This is a relatively small flow for Ísafjörður, as it did

395   not reach the fjord nor the man-made drainage channel on the lower part of the slope.

396   Despite debris flows 3DF, 2DF, and 4DF being older flows (hence more eroded), the

397   patterns in deposition and erosion are preserved. We can therefore analyse patterns of erosion

398   and deposition in all the flows together using the methods described in section 2.4. Figure 6

399   shows a box-plot showing normalised representative deposition (Fig. 6A) and erosion (Fig.

400   6B) thickness against slope as a compilation of data for all the debris flows. Using Fig. 6, we

401   can then compare the onset of deposition and cessation of erosion in these flows with those

402   found by other authors for hillslope flows. Note that the extension of the boxes above the

403   zero-line in Fig. 6A (marked X) at slope angles > 43° is an artefact because of the protrusion

404   of bedrock surfaces in the alcoves of debris flows 2DF and 3DF above the interpolated

405   surfaces.

406

407   **[Fig. 6 here]**

408

409   Our results are interesting in that we find measurable deposition at slope angles of 37°.

410   This is higher than reported by previous studies. Lorente et al. (2003) reported 17.8° as the

411   onset slope for deposition; and Fannin and Wise (2001) reported unconfined (hillslope) flows

412   as depositing at angles < 18.5° on average in the Queen Charlotte Islands, British Columbia,

413   Canada, but their data show deposition occurring up to 38º in some cases (it is not clear,

414   however, if these flows are exclusively hillslope debris flows). However, Larsson (1982)

415   reported deposition at as much as 35° for debris flows in Longyear Valley, Spitsbergen,

416   Norway. Matthews et al. (1999) reported deposition on slopes of up to 25º in Leirdalen,

417   Jotunheimen, Norway; and Rapp and Nyberg (1981) reported deposition on 30° slopes in

418   Nissunvagge, Sweden. For confined flows, deposition does not begin until much lower slope

419   angles are reached on the fan (e.g., Staley et al., 2006; Prochaska et al., 2008). Hence, for the

420   flows studied in this paper, deposition consistently begins at a much higher average slope

421   angle than reported by the majority of other authors.

422   Fannin and Wise (2001) reported their lowest limit of erosion on average as being 18.5°

423   for unconfined flows, but this lower limit has not been widely reported elsewhere in the

424   literature. From Figs. 6B and 5, apparently a lower slope erosion threshold exists of ~ 19° for

425   debris flows in our study, marked by the vertical line in Fig. 6B. This is reinforced by field

426   observations of erosion occurring near the distal end of the debris flow coincident with an

427   increase in local slope as shown in Fig. 7. It is also consistent with the observation of *insitu*

428   grass between the levees of debris flow 5DF at a sudden decrease in slope below 19°. This

429   phenomenon has been noted by other authors in other locations (Rapp, 1960; Matthews et al.,

430   1999; Luckman, 1992), but not quantified.

431

432   **[Fig. 7 here]**

433

434   **4. Data analysis**

435   *4.1. Comparison with previous empirical relationships for debris flow total travel distance*

436   Rickenmann (1999) used data from 232 confined debris flows from around the world to

437   derive the following relationships:

438
$$L = 30(MH_e)^{0.25} \qquad (1)$$

439
$$L = 1.9M^{0.16}H_e^{0.83} \qquad (2)$$

440   where L is the total travel distance, H_e is the elevation difference between the source and the

441   lowest point of deposition, and M is the magnitude or total volume. Equation (1) is a

442   theoretical relationship between distance travelled and energy potential (MH_e), and the

443   constant has been selected to approximate average total travel distance in the data of

444   Rickenmann (1999). Equation (2) is the regression equation of L, M, and H_e that best fits

445   Rickenmann's (1999) data. Similarly, Lorente et al. (2003) compiled data from 961

446   unconfined debris flows in the Flysch sector of central Spanish Pyrenees to derive the

447   following relationships:

448
$$L = 7.13(MH_e)^{0.271} \qquad (3)$$

449
$$L = -12.609 + 0.568h + 0.412s \qquad (4)$$

450   where h is the elevation difference between the source and the starting point of deposition,

451   and s is the average gradient of the source area in degrees. Lorente et al. (2003) used Eq. (1)

452   as the basis for Eq. (3), but adjusted both the exponent and the constant to fit their data.

453   Equation (4) is the result of a linear regression of the variables that had the highest correlation

454   with total travel distance from Lorente et al.'s (2003) data.

455

456   **[Fig. 8 here]**

457

458   For Rickenmann's (1999) Eq. (1), debris flow 1DF lies well above the line $x = y$ in Fig.

459   8, which means its total travel distance is shorter than that predicted by this relationship.

460   Using Rickenmann's (1999) Eq. (2), our debris flows 1DF, 10DF, and 8DF all lie well above

461   the $x = y$ line and therefore have a shorter total travel distance than predicted. This is because

462   the elevation difference is more important in Eq. (2) than (1), giving a longer predicted total

463   travel distance for 8DF and 10DF, which have greater elevation differences. For both the

464   Rickenmann (1999) relationships (Eqs. 1 and 2), our debris flows 2DF, 3DF, 5DF, and 7DF

465   lie close to the $x = y$ line: the measured total travel distances match the predicted ones quite

466   well. All the debris flows in this study lie well below the line for both of the relationships

467   from Lorente et al. (2003), i.e., all the flows we have studied have larger total travel distances

468   than would be predicted by Lorente et al. (2003). Existing relationships do not seem to fit our

469   results very well, so we now proceed to develop our own empirical model in the following

470   sections.

471   *4.2. Derivation of an empirical relationship for hazard prediction*

472   By treating cumulative packets of the segmented debris flows from top to bottom as

473   progressively larger subsamples of the main debris flow, we noticed predictable patterns in

474   the pattern of deposition. Figure 9 shows a plot of cumulative average slope against

475   cumulative normalised deposition thickness. Cumulative average slope (θ_n) was calculated

476   for each segment **n** as follows:

477
$$\theta_n = \frac{\sum_{i=0}^{n} S_i}{n} \tag{5}$$

478   where S_i is the slope within segment i, and n is the number of segments counted from the

479   source of the flow downward. The cumulative normalised deposition thickness (Z_n) was

480   calculated for each segment n as follows:

481
$$Z_{,n} = \sum_{i=0}^{n} \frac{Z_{,i}}{Z_T}$$
(6)

482   where Z_i is the representative thickness for that segment, and Z_T is the sum of the

483   representative thicknesses for all segments in the debris flow.

484

485   **[Fig. 9 here]**

486

487   All the debris flows studied fall within a narrow range of cumulative average slope for

488   a given representative thickness, and most have an initial steep section over which no

489   deposition occurs. Deposition then begins at a cumulative average slope of 35-40°. The

490   behaviour of the debris flows then falls into one of three groups: (i) those which then deposit

491   linearly for the rest of their length (debris flows DF2, DF3, and DF7), (ii) those with a sudden

492   decrease in deposition before their terminus (debris flows DF1 and DF8), and (iii) those

493   which show strong initial deposition that tails off into a constant rate of deposition at lower

494   slope angles (debris flows 5DF and 10DF). We can use these relationships to generate best-fit

495   curves, allowing us to predict potential future flow behaviour.

496   *4.3. Creating a hazard map from empirical relationships*

497   Enough consistency exists in the relationship between cumulative average slope and

498   cumulative normalised deposition thickness to fit curves to the envelope of the data points

499   shown in Fig. 9 (this process is described more fully in Appendix B). We have fitted three

500   types of curves (Fig. 9): linear (on the lower boundary, labelled 2 in Fig. 9), sigmoidal

501   (Boltzmann-family, to the highest average slope, labelled 3 in Fig. 9 and lowest average

502   slope, labelled 4 in Fig. 9), and exponential (to the average, labelled 1 in Fig. 9). These

503   curves represent the patterns in behaviour labelled (i), (ii), and (iii) described in section 4.1,

504   respectively. We have then modelled the debris flow behaviours based on these curves along

505   19 simulated debris flow tracks (Fig. 10). The tracks were generated from the lines of greatest

506 fluid accumulation as derived from hydrological modelling of the LiDAR DEM using Arc

507 Hydro Tools 9.0. Centrelines were digitised from this accumulation model and then split or

508 segmented at 5-m intervals, as per the empirical model (see Fig. 3). The underlying slope for

509 each of these segments was extracted from the DEM. These models require two inputs in

510 addition to the flow paths: the planimetric area and the debris flow volume.

511   As debris flow 1DF was a relatively small event compared to those in 1999, we used its

512 volume and planimetric area as an end member to estimate the thickness of deposits reaching

513 the town on a set of 19 tracks shown in Fig. 10. The results of this modelling show that for

514 models 2 and 4 upper parts of the town would be at risk from any debris flow; and for models

515 1 and 3 the flows do not have sufficient mobility to reach the town, no matter what the input

516 volume and area. To demonstrate how the thicknesses change with increasing volume (and

517 planimetric area), the thicknesses of debris reaching the town are tabulated for different input

518 parameters for three example flow-paths (labelled on Fig. 10 Model 1) for all four models in

519 Table 6. The results from 1 and 3 emphasise that these types of flows rarely have sufficient

520 mobility to reach the town, no matter what the input volume and area are for these two

521 models.

522

523 **[Fig. 10 here]**

524

525 **5. Discussion**

526 *5.1. Reliability of volume data*

527   Our method of estimating pre-flow surfaces has been tested on the debris flows for

528 which we do have pre-flow data (7DF, 8DF, and 10DF), it seems to underestimate deposition

529 volumes and greatly over-estimate erosion volumes (Table 4). We do not have a debris flow

530 $> 1000 \text{ m}^3$ on which we can test this method, but it is likely that the percentage difference in

531 calculating the deposition volume by this method would decrease with greater volume, as the

532 absolute differences would increase only slowly. It is also likely that the percent difference in

533 erosion volume would remain large, as the kriging is performed over larger source areas,

534 leading to the absolute difference increasing with the volume.

535   However, the interpolation on accurate GPS and LiDAR elevation data gives realistic

536 ranges of volumes for these flows. Considering the inherent bias towards underestimation, the

537 volume estimates are larger than previous estimates for this area: our "medium" flow 1DF

538 has a volume of about 8000 m^3 compared to 3000 m^3 calculated by Decaulne et al. (2005) for

539 a "large" debris flow 2DF in 1999 (Table 5). We have used several different methods to

540 calculate the deposition volumes of 1DF and have found that all the results are consistent

541 (Table 5). Debris flow 1DF is a medium-sized flow for this region, and the results are within

542 realistic bounds for this scale of flow (Innes, 1983). However, debris flow 1DF has the largest

543 errors from lack of pre-flow data, and hence all other flows are better constrained and have

544 more reliable volume estimates.

545 *5.2. Patterns in deposition and erosion*

546   Debris flows 1DF and 5DF show morphological evidence of the pulsing nature of debris

547 flows in the patterns of their deposits. The break-off lobe in 1DF is probably a result of the

548 first pulse, which was able to break over the preexisting levees at the bend in the channel

549 (Fig. 5B – just above II). Later pulses blocked this path with their own levees and continued

550 down the path of previous flows. For debris flow 5DF, a major peak in deposition is located

551 about 50 m from the end of the flow (Fig. 5A – III); this was also probably an original

552 terminal lobe before a later pulse broke out through a levee above it. This later pulse formed

553 small levees and then spread out into a sheet deposit, suggesting a higher mobility and, hence,

554 water content. This demonstrates that a debris flow does not necessarily follow the line of

555 greatest initial slope, but that earlier pulses can block further flow; this divagation behaviour

556 of debris flows has been described by several other authors from deposits (e.g., Addison,

557 1987; Morton et al., 2008) and modelling (Zanuttigh and Lamberti, 2007). These field

558 observations also point to the variable composition of the pulses that form a debris flow

559 event. Although our model does not incorporate these observations explicitly, we use the

560 knowledge of this pulsing nature to expand and inform conclusions based on model results.

561   Debris flows continue to be mobile at low slope angles, with debris being transported at

562 slope angles as small as 7-10°, although initiation seems to require a high slope angle (> 40°).

563 We have measured little deposition at lower slope angles, and several possible reasons exist

564 for this:

565   (i) The debris flows studied here exhausted the available material before reaching low

566   slopes. We have not studied any very large, fresh flows that could perhaps continue

567   depositing at low slope angles, as their material is not exhausted by deposition on

568   higher slopes.

569   (ii) Any low-slope deposits within Ísafjörður or on roads remaining from historical flows

570   would almost certainly have been cleared away.

571   (iii)Urbanisation on low slopes prevents debris flows from progressing unimpeded

572   downslope.

573   (iv)Morphology of the slopes in Ísafjörður means that very low (<< 10°) slope angles are

574   not abundant above the shoreline.

575 Previous studies (Decaulne, 2001) have suggested that deposition of lobes does occur at these

576 low slope angles, but it is unclear if the water content is low enough within these mobile

577 flows to maintain levees.

578   The ideal slope angles for deposition appear to be around 25°, enabling the outer edge

579 of the flow to stabilise into levees while the main body of the flow remains mobile.

580 Deposition begins to occur at much higher slope angles than reported for previous flows (e.g.,

581 Coe et al., 1997; Lorente et al., 2003). This potentially indicates that the flow deposits in the

582 Ísafjörður region have a higher angle of dynamic friction or a higher viscosity (possibly

583   related to lower water content or higher clay content) than previously reported for debris

584   flows. This is supported by field observations that the levees are able to maintain high

585   external and internal slopes.

586   In the study area a threshold slope of 19° is observed, below which erosion completely

587   ceases. Whenever this threshold is exceeded lower down the flow, erosion begins again as

588   shown in Fig. 7. This means that the debris flows are probably bulking (i.e., incorporating

589   material eroded from along the flow path) as they progress downslope, although we were not

590   able to estimate the amount of bulking, because of a lack of reliable data in the source areas.

591   *5.3. Comparison with previous empirical relationships for debris flow total travel distance*

592   Figure 8 shows how the debris flows studied here compare with empirical

593   relationships for debris flow run-out distances derived by Rickenmann (1999) and Lorente et

594   al. (2003).

595   The debris flows studied here fit best with the confined debris flows (Equation 1)

596   studied by Rickenmann (1999), but the total travel distance is greater than predicted from the

597   hillslope debris flows studied by Lorente et al. (2003) in Flysch in the Pyrenees. This is

598   surprising as the debris flows in our study area most closely resemble those of Lorente et al.

599   (2003), being unconstrained hillslope flows rather than the confined torrent debris flows of

600   Rickenmann (1999).

601   From this we infer that the larger debris flows in our area are generally more mobile

602   than hillslope flows studied by Lorente et al. (2003), but less mobile than confined flows

603   studied in a wide range of settings by Rickenmann (1999). However, the smaller flows have

604   about the same mobility as Rickenmann's (1999) channelized flows. The higher mobility of

605   these flows seems counter-intuitive considering their higher angle of dynamic friction or

606   higher viscosity implied by observed high levee slopes and deposition at high local slope

607   values (detailed in sections 3.1 and 3.3). However, Iverson (1997) concluded that the

608   structure of the deposits does not reflect the properties of the original debris flow, and the

609 interplay of the flow's viscosity with the fluid and granular parts of the flow is poorly

610 understood (Iverson, 1997). We hypothesise that the high mobility compared to Lorente et

611 al. (2003) is a reflection of the larger scale of the debris flows in this study. Clearly, the

612 flows in our area do not closely match existing empirical relationships. We conclude that

613 empirical prediction from simple models is insufficient here; and that without the application

614 of more complex models, the prediction of future flow lengths in a given area can only be

615 made by the analysis of detailed measurements of previous flows from the selected area. Here

616 we present an example of how this can be implemented.

617 *5.4. Developing a new empirical model for debris flow prediction*

618   For the debris flows studied in the Westfjords, the relationship between slope and

619 deposition does not strongly depend on the overall mass nor the source material's grain size,

620 grain size distribution, or angularity (detailed in section 3.1). All the flows show similar basic

621 patterns yet have different masses (Table 4) and comprise different materials (Fig. 4, and

622 section 3.1). Both field observations and analysis of the isopach and slope profiles (Fig. 5)

623 point to a strong relationship between slope and deposition-erosion volume. From the isopach

624 data, we have derived a predictive relationship for flows in this area. Figure 9 shows the data

625 and trends in cumulative slope and normalised deposition thickness, as derived in section 4.1

626 and Appendix B, which lead to this predictive relationship. As mentioned in section 4.1,

627 debris flows 2DF, 3DF, and 7DF do not have the sudden drop in deposition at low cumulative

628 slope that is shown by most of the other flows. However, we believe that this is not a feature

629 of the flow mechanics but a result of the deposits being later removed by anthropogenic

630 mechanical excavation (section 3.1). This removal has affected the normalisation in Fig. 9,

631 but we estimate that these deposits make up an insignificant fraction of the total deposition

632 volume and therefore would not push these flows outside the main data envelope. We

633 attribute the other differences between debris flows in Fig. 9 to gross rheological differences

634 and to the variation in rheology of their constituent pulses. These differences are surprisingly

635 small, however, considering the variation in topographical setting, source of material, fines

636 content, clast size, angularity, and grain size distribution between the flows.

637   The data in Fig. 9 form a discrete envelope that describes the way in which we expect a

638 debris flow to evolve in terms of proportion of overall deposit thickness and hence volume

639 with cumulative slope. Therefore, with a starting volume, planimetric area, and a DEM, this

640 relationship can be used to predict overall total travel distance and deposit thickness at a

641 given location.

642 *5.5. Predicting hazard*

643   We have used the empirical relationships described in section 5.4 to simulate debris

644 flow deposition and overall total travel distance along synthetic flow paths as explained in

645 section 4.2. Different flow behaviours are represented by the four models shown in Fig. 9,

646 and these have been simulated along the synthetic tracks. Models 2 and 4 always reach the

647 houses no matter what the starting volume (Table 6; Fig. 10). Models 1 and 3 never reach the

648 houses, and again this is independent of starting volume (Table 6: Fig. 10). As noted in

649 section 5.4, debris flows 2DF, 3DF, and 7DF do not have the sudden drop in deposition at

650 low cumulative slope that is shown by most of the other flows; and these flows form the basis

651 for creating model 1 (exponential). Hence, we can discount this model as being unrealistic

652 for most debris flows. The sigmoidal (Boltzmann) models 3 and 4 seem to represent the

653 inherent behaviour of most of the flows: an initial slow increase in deposition, a stable middle

654 area with approximately constant deposition, and a sharp drop-off at low slope angles.

655 However, the difference in terms of overall deposit thickness is not great between models 2

656 (linear) and 4 (sigmoidal), hence a simple linear model would suffice to implement this

657 method, without the need to fit a precise curve any particular flow.

658   Protective ditches have been dug above the town of Ísafjörður in two locations (marked

659 in Fig. 2) to protect the population and houses from debris flows. In our modelled flows, the

660 flow thickness only matches the depth of the protective ditches (i.e., the flow only progresses

661   past the ditches) when the flow is extremely large in volume ($> 100\,000$ m^3 is an

662   exceptionally large flow for this region). We should note that in reality the ditches were

663   nearly overwhelmed (mud and water reached the houses) in 1999 (Decaulne et al., 2005) by

664   2DF and 3DF, which have estimated volumes of 3000 and 1000 m^3, respectively (Table 5).

665   We note that the ditches have since been widened (Decaulne, 2007). However, our model

666   results show that medium-sized debris flows result in greater than 1 m of deposits at the

667   eastern ditch, so two medium flows occurring close to one another in time and space would

668   overwhelm this ditch and flows would reach the houses. Given that debris flows can be

669   triggered simultaneously (e.g., Coe et al., 2007; Decaulne and Sæmundsson, 2007), this

670   appears to be a plausible hazard. However, the frequency of occurrence of these multiple

671   events is unknown for Ísafjörður, so we assume that this would be a comparatively rare event,

672   but severe if it does occur. This analysis has enabled us to identify areas of the town at risk

673   that would not be obvious otherwise. To prioritise any mitigation work done by the

674   authorities, this model could be combined with estimates of most likely flow areas based on

675   historical data and cost-benefit considerations. For example, although the electricity

676   substation is unprotected, damage to it although inconvenient is unlikely to cause loss of life,

677   compared to residential properties.

678   Our model does not take into account the effect of the relative timings of multiple

679   events nor the number of pulses in a single flow event. For example, a medium-sized flow

680   could occur in a single pulse and stabilise on the slope with the terminal lobe at the ditch and

681   rest of debris backed up behind it. However, such an event could also have many pulses, the

682   first of which fills the ditch allowing the next pulses to ride over the top. These hypothetical

683   events could have the same overall volume but very different outcomes. In addition, the flow

684   paths we have used in our model run down the steepest slope, but as noted previously,

685   (sections 3.1 and 3.3) debris flows do not necessarily conform to this path. However, the flow

686   routes we have produced are representative of the slopes experienced by a debris flow as it

687   progresses and therefore can be used as an indication of thickness of deposits expected for the

688   flow, if not the exact path line.

689   Our model is an oversimplification of the behaviour of the flow, but it is conservative in

690   its simplifications. The advantage of this model is that it meets the conditions of Hurlimann et

691   al. (2008), which are (i) the method must specify a spatial distribution, and results must cover

692   the entire study area; (ii) the method applied should be able to incorporate different volumes

693   as input data; and (iii) the output of the method should enable intensity determination without

694   the need for the time and expense of a full two-dimensional flow model, requiring back-

695   calculation to determine rheology and selection of the most appropriate flow-resistance law.

696   Our model has a similar philosophy in this respect to Fannin and Wise (2001), although their

697   model required the additional inputs of length, width, and azimuth of each reach in the debris

698   flow. Their model also dealt with transitional and confined debris flows in addition to

699   unconfined debris flows and also included bulking (incorporation of material eroded along

700   the flow path). Except bulking, none of these additional factors are of importance in purely

701   hillslope flows.

702

703   **6. Conclusions**

704   (i) The length and pattern of deposition of a future debris flow of given volume can be

705   estimated from slopes measured on DEMs of its predicted flow path. This conclusion

706   is based on the fact that debris flows above Ísafjörður, in Hnífsdalur and in

707   Súgandafjörður, consistently showed similar relationships between cumulative

708   average slope and normalised deposition thickness, despite each flow having wide

709   differences in source materials and setting. This has allowed us to identify areas of

710   the town of Ísafjörður previously not acknowledged as being at risk. We recommend

711   areas that have been identified as medium risk or above do not undergo future

712   development. We suggest that future work should include testing this model with

713   additional data and extending it in to other areas.

714   (ii) . This model is notable for its simplicity, which allows future debris flow

715   characteristics to be predicted without the need to determine the precise fluid dynamic

716   parameters of the flow such as viscosity and velocity, which are required to

717   implement more complex models.

718   (iii)We have found that erosion occurs when slope angles are > 19° in any part of the

719   flow. Hence, any new development should be located in areas with slopes much less

720   than this, in addition to being located away from areas highlighted as medium to high

721   risk in the debris flow modelling.

722   (iv)Satisfactory estimates of debris flow volumes can be derived from well-placed cross

723   profiles, as demonstrated by other authors, however patterns in erosion and deposition

724   cannot be analysed using this method.

725   (v) Our method of estimating volumes using Krige algorithm produces reasonable

726   estimates of debris flow deposition volume, even when pre-flow data are absent.

727   When pre-flow data are absent the deposition volume tends to be underestimated and

728   the erosion volume greatly over-estimated, but the patterns in deposition and erosion

729   are preserved and realistic bounds of error are given by this method.

730   (vi)Large hillslope-style debris flows above Ísafjörður, in Hnífsdalur and in

731   Súgandafjörður, do not fit existing empirical models based on channelized torrent-fan

732   systems or hillslope flows. Given their significant hazard potential, they therefore

733   warrant more study. Furthermore, an extended study of the cessation point of erosion

734   and the onset threshold of deposition in hillslope debris flows in other regions could

735   lead to more generally applicable relationships, which in turn could provide an

736   important link between the morphometric properties of debris flow deposits and the

737   fluid dynamics of the flows themselves.

738 **Acknowledgements**

Appendix A – Analysis of Errors

Table 2 summarises the main sources of error in the data collection and data processing chain. The improvement in the accuracy of the LiDAR data through matching the tracks using LS3D (Akca, 2007a, b) is clearly shown. The errors associated with data collection (with the exception of LiDAR data preprocessing) are very small compared to the errors generated in interpolating the data. This must be taken into consideration when interpreting the total volume estimates. The best volume estimate would be from a surface that had densely spaced points both before and after a debris flow occurs (both preferably from corrected LiDAR data). Given the financial costs associated with collecting LiDAR data and the unpredictable nature of debris flows, the systematic collections of such data is unlikely.

The errors from the upper and lower interpolated surfaces were combined using the standard formula:

$$\sigma_Z = \surd(\sigma_A{}^2 + \sigma_B{}^2) \tag{A1}$$

where σ_Z is the total uncertainty, and σ_A and σ_B are the uncertainties of the two surfaces. These errors vary spatially and can become large away from data points.

Appendix B – Model Production

This appendix describes the method by which the curves in Fig. 9 were generated; "*x*"
refers to cumulative average slope and "*y*" refers to cumulative deposition thickness. The
parameters derived from the least squares fits described in this appendix, along with their
associated errors, are given in Table 7. The equations used to generate the model curves
shown in Fig. 9 are as follows (with numbering here in the same sequence as in Fig. 9):

$$0.03 + 1876170 \text{ x } e^{(-x/2.217)} \tag{B1}$$

$$(36 - x) / 8.5 \; (36 - 8.5x) \tag{B2}$$

$$-0.03816 + 1.04016 / (1 + e^{((x - 36.30119)/1.00308)}) \tag{B3}$$

$$1.012 / (1 + e^{((x - 32)/1.00308)}) \tag{B4}$$

The shape of Eq. (B1) was derived by performing least squares fit of

$$y = A + B * e^{(-x/C)} \tag{B5}$$

on the data from debris flow 2DF. The χ^2 value for the fit is 0.00547, which implies a
significant *p*-value of $<< 0.001$. The r^2 value is 0.93652.

Linear regression of the data from debris flow 5DF was used to derive Eq. (B2) using
the following relation:

$$y = A + Bx \tag{B6}$$

The r^2 value of this fit is 0.854663, which gives a significant *p*-value of $<< 0.0001$.

The curves from Eqs. (B3) and (B4) were derived by performing a least squares fit of

$$y = A + (B - A) / (1 + e^{((x - C)/D)}) \tag{B7}$$

788   using data from debris flow 1DF. The χ^2 value for the fit is 0.00027, which implies a

789   significant *p*-value of $\ll 0.001$ and the I value of 0.99828. Equation (B4) is a translation of

790   Eq. (B3) along the x-axis, an estimate of the lower limit of the data envelope.

791 **10. References**

792 Addison, K., 1987. Debris flow during intense rainfall in Snowdonia, North Wales: A
793   preliminary survey. Earth Surface Processes and Landforms 12(5), 561-566.

794 Akca, D., 2007a. Least squares 3d surface matching, Eidgenössische Technische Hochschule
795   Zürich, Zürich, 92 pp.

796 Akca, D., 2007b. Matching of 3d surfaces and their intensities. ISPRS Journal of
797   Photogrammetry and Remote Sensing 62(2), 112-121.

798 Arnalds, Þ., Sauermoser, S., Jóhannesson, T., Grímsdóttir, H., 2002. Hazard zoning for
799   Ísafjörður and Hnífsdalur, Technical Report VÍ-ÚR15, Veðurstofa Íslands, Reykjavík.

800 Arnalds, Þ., Jónasson, K., Sigurðsson, S., 2004. Avalanche hazard zoning in Iceland based on
801   individual risk. Annals of Glaciology 38, 285-290.

802 Ballantyne, C.K., Benn, D.I., 1994. Paraglacial slope adjustment and resedimentation
803   following recent glacier retreat, Fabergstolsdalen, Norway. Arctic and Alpine
804   Research 26(3), 255-269.

805 Berti, M., Simoni, A., 2007. Prediction of debris flow inundation areas using empirical
806   mobility relationships. Geomorphology 90, 144-161.

807 Breien, H., De Blasio, F.V., Elverhøi, A., Høeg, K., 2008. Erosion and morphology of a
808   debris flow caused by a glacial lake outburst flood, western Norway. Landslides 5(3),
809   271-280.

810 Carrara, A., Crosta, G., Frattini, P., 2008. Comparing models of debris-flow susceptibility in
811   the alpine environment. Geomorphology 94, 353-378.

812 Casali, J., Loizu, J., Campo, M.A., De Santisteban, L.M., Alvarez-Mozos, J., 2006. Accuracy
813   of methods for field assessment of rill and ephemeral gully erosion. Catena 67(2),
814   128-138.

815 Clague, J.J., Evans, S.G., Blown, I.G., 1985. A debris flow triggered by the breaching of a
816   moraine-dammed lake, Klattasine Creek, British Columbia Canadian Journal of Earth
817   Sciences 22(10), 1492-1502.

818 Coe, J.A., Glancy, P.A., Whitney, J.W., 1997. Volumetric analysis and hydrologic
819   characterization of a modern debris flow near Yucca Mountain, Nevada.
820   Geomorphology 20(1-2), 11-28.

821 Coe, J.A., Godt, J.W., Wait, T.C., Kean, J.W., 2007. Field reconnaissance of debris flows
822   triggered by a july 21, 2007, thunderstorm in Alpine, Colorado, and vicinity. Open-
823   File Report 2007-1237, U.S. Geological Survey.

824 Decaulne, A., 2001. Dynamique des versants et risques naturels dans les fjords d'Islande du
825   nord-ouest l'impact geomorphique et humain des avalanches et des debris flows. PhD
826   Thesis, Université Blaise Pascal, Clérmont-Ferrand, 263 pp.

827 Decaulne, A., Sæmundsson, Pétursson, O., 2005. Debris flow triggered by rapid snowmelt: A
828   case study in the Gleiðarhjalli area, northwestern Iceland. Geografiska Annaler Series
829   A-Physical Geography 87A(4), 487-500.

830 Decaulne, A., 2007. Snow-avalanche and debris-flow hazards in the fjords of north-western
831   Iceland, mitigation and prevention. Natural Hazards 41(1), 81-98.

832 Decaulne, A., Sæmundsson, 2007. Spatial and temporal diversity for debris-flow
833   meteorological control in subarctic oceanic periglacial environments in Iceland. Earth
834   Surface Processes and Landforms 32, 1971-1983.

835 Fannin, R.J., Wise, M.P., 2001. An empirical-statistical model for debris flow travel distance.
836   Canadian Geotechnical Journal 38(5), 982-994.

837 Favalli, M., Fornaciai, A., Pareschi, M.T., 2009. Lidar strip adjustment: application to
838   volcanic areas. Geomorphology, in press.

839 Gabet, E.J., Bookter, A., 2008. A morphometric analysis of gullies scoured by post-fire
840   progressively bulked debris flows in southwest Montana, USA. Geomorphology 96(3-
841   4), 298-309.

842 Gardner, J.S., 1989. High magnitude geomorphic events in the Canadian rocky mountains.
843   Studia Geomorphologica Carpatho-Balcanica 23, 39-51.

844 Gartner, J.E., Cannon, S.H., Santi, P.M., Dewolfe, V.G., 2008. Empirical models to predict
845   the volumes of debris flows generated by recently burned basins in the western U.S.
846   Geomorphology 96(3-4), 339-354.

847 Hurlimann, M., Rickenmann, D., Medina, V., Bateman, A., 2008. Evaluation of approaches
848   to calculate debris-flow parameters for hazard assessment. Engineering Geology
849   102(3-4), 152-163.

850 Innes, J.L., 1983. Debris flows. Progress in Physical Geography 7, 469-501.

851 Iverson, R.M., 1997. The physics of debris flows, Reviews of Geophysics, pp. 245-296.

852 Iverson, R.M., Schilling, S.P., Vallance, J.W., 1998. Objective delineation of lahar-
853   inundation hazard zones. Bulletin of the Geological Society of America 110(8), 972-
854   984.

855 Jakob, M., 2005. A size classification for debris flows. Engineering Geology 79(3-4), 151-
856   161.

857 Johnson, A. M., J. R. Rodine, 1984. Debris flow. In: Brundsen, D., Prior, B. (Eds.), Slope
858   Instability. John Wiley, Hoboken, NJ, pp. 257-361.

859 Kanji, M.A., Cruz, P.T., Massad, F., 2008. Debris flow affecting the Cubatão oil refinery,
860   Brazil. Landslides 5(1), 71-82.

861 Larsson, S., 1982. Geomorphological effects on the slopes of Longyear valley, Spitsbergen,
862   after a heavy rainstorm in July 1972. Geografiska Annaler Series A-Physical
863   Geography 64(3-4), 105-125.

864 Lorente, A., Beguería, S., Bathurst, J.C., García-Ruiz, J.M., 2003. Debris flow characteristics
865   and relationships in the central Spanish Pyrenees. Natural Hazards and Earth System
866   Science 3(6), 683-692.

867 Luckman, B.H., 1992. Debris flows and snow avalanche landforms in the Lairig Ghru,
868   Cairngorm Mountains, Scotland. Geografiska Annaler Series a-Physical Geography
869   74(2-3), 109-121.

870 Matthews, J.A., Shakesby, R.A., McEwen, L.J., Berrisford, M.S., Owen, G., Bevan, P., 1999.
871   Alpine debris-flows in Leirdalen, Jotunheimen, Norway, with particular reference to
872   distal fans, intermediate-type deposits, and flow types. Arctic Antarctic and Alpine
873   Research 31(4), 421-435.

874 Morton, D.M., Alvarez, R.M., Ruppert, K.R., Goforth, B., 2008. Contrasting rainfall
875   generated debris flows from adjacent watersheds at forest falls, southern California,
876   USA. Geomorphology 96(3-4), 322-338.

877 Norðdalh, H., 1990. Late Weichselian and early Holocene deglaciation history of Iceland.
878   Jökull 40, 27-50.

879 Okuda, S., 1989. Recent studies on rapid mass movement in Japan with reference to debris
880   hazards. Studia Geomorphologica Carpatho-Balcanica 23, 5-22.

881 Prochaska, A.B., Santi, P.M., Higgins, J.D., Cannon, S.H., 2008. Debris-flow runout
882   predictions based on the average channel slope (ACS). Engineering Geology 98(1-2),
883   29-40.

884 Rapp, A., 1960. Recent development of mountain slopes in Kärkevagge and surroundings,
885   northern Scandinavia. Geografiska Annaler Series A-Physical Geography 42(2-3), 65-
886   200.

887 Rapp, A., Stromquist, L., 1976. Slope erosion due to extreme rainfall in the Scandinavian
888   mountains. Geografiska Annaler Series a-Physical Geography 58(3), 193-200.

889 Rapp, A., Nyberg, R., 1981. Alpine debris flows in northern Scandinavia - morphology and
890   dating by lichenometry. Geografiska Annaler Series A-Physical Geography 63(3-4),
891   183-196.

892 Rickenmann, D., 1999. Empirical relationships for debris flows. Natural Hazards 19(1), 47-
893   77.

894 Santi, P.M., deWolfe, V.G., Higgins, J.D., Cannon, S.H., Gartner, J.E., 2008. Sources of
895   debris flow material in burned areas. Geomorphology 96, 310–321.

896 Scheidl, C., Rickenmann, D., Chiari, M., 2008. The use of airborne LiDAR data for the
897   analysis of debris flow events in Switzerland. Natural Hazards and Earth System
898   Sciences 8, 1113–1127.

899 Staley, D.M., Wasklewicz, T.A., Blaszczynski, J.S., 2006. Surficial patterns of debris flow
900   deposition on alluvial fans in Death Valley, CA using airborne laser swath mapping
901   data. Geomorphology 74(1-4), 152-163.

902 Wilkerson, F.D., Schmid, G.L., 2008. Distribution of debris flows in Glacier National Park,
903   Montana, U.S.A. Journal of Mountain Science 5(4), 318-326.

904 Zanuttigh, B., Lamberti, A., 2007. Instability and surge development in debris flows.
905   Reviews of Geophysics 45(3) .

Figure legends

Fig. 1. Inset: Map of Iceland showing location of main image (thick grey box). Main:

hillshade representation of the NERC ARSF's LiDAR data collected in 2007 for

Súgandafjörður and Skutulsfjörður, with locations in Fig. 2 marked A, B, C.

Fig. 2. Air photographs of the study area obtained by NERC ARSF in 2007, with debris

flows in this study marked with black outlines. Contours are at 20-m intervals. (A) Debris

flows 8DF and 10DF are located on the east side of Súgandafjörður, north of Botn on the

road to Selárdalur. (B) Debris flow 5DF is located to the south of Hnífsdalur above the valley

road. (C) Debris flows 1DF, 2DF, 3DF, 4DF, and 7DF are located above the town of

Ísafjörður, sourced from the Gleiðarhjalli bench. White arrows indicate the extents of the two

main drainage ditches mentioned in the text.

Fig. 3. A schematic oblique three-dimensional illustration of how analysis was performed by

segmenting the debris flows along-track. This figure shows debris flow 1DF, which has been

split into segments 5 m wide at the channel centre-line. Summary statistics were derived for

each of the segments from underlying data sets, such as isopach maps of erosion, deposition,

and an underlying DEM.

Fig. 4. (A-C) Maps of the spatial relation between erosion and deposition as derived by

differencing the LiDAR generated topography from the post-flow DEM for debris flows

10DF, 8DF, and 7DF, respectively. (A'-C') Maps for the same flows, however, the base-

topography used for differencing was derived by Krige interpolation over the area of the

debris flow (method described in section 2.3).

931   **Fig. 5.** (A) Long profile and isopach map of debris flow 5DF. (B) Long profile and isopach

932   map of debris flow 1DF. Contours on the isopach maps are at 5-m spacing. MA10 in the long

933   profiles is the abbreviation for Moving Average over 10 data points. Black points correspond

934   to elevation on the right-hand axis, and pink/blue points correspond to slope represented on

935   the right-hand axis.

936

937   **Fig. 6.** Box-plots showing the distribution of normalised representative deposition thickness

938   (A) and representative erosion thickness (B) thickness plotted in 2° slope bins. Normalised

939   thickness is calculated by taking the thickness of the flow in a given segment and dividing it

940   by the total thickness for all segments (described in detail in section 2.4). All data from all

941   debris flows are included. The boxes represent the first and the third quartiles of the

942   distribution, with the black bar marking the median. The narrow bars mark the maximum and

943   minimum of the distribution, with the circle symbols representing "mild" outliers (between

944   1.5 and 3 interquartile ranges beyond the bars) and the stars representing "extreme" outliers

945   (above 3 interquartile ranges beyond the bars). The erosion slope threshold of 19° is marked

946   by a vertical line in (B). In (A), X marks the region where data are artefacts from the

947   interpolation technique, rather than a true signal. This problem occurred within the alcoves.

948

949   **Fig. 7.** (A) The base of the northernmost debris flow sourced from Gleiðarhjalli bench. (B)

950   The base of debris flow 4DF. White arrows indicate the extent of the eroded channels. (C)

951   Large black arrows indicate locations of photos (A) and (B) on a slope map of the 5-m DEM,

952   with small black arrows showing increases in local slope that correspond to erosional sections

953   picked out by the white arrows in (A) and (B).

954

955   **Fig. 8.** Plot of the total travel distance predicted for the debris flows in this study by the

956   empirical relationships derived by Rickenmann (1999) and Lorente et al. (2003), against our

957   measured total travel distance for the same debris flows. Rickenmann-1 refers to the

958   relationship given in Eq. (1); Rickenmann-2 to Eq. (3); Lorente-1 to Eq. (3), and Lorente-2 to

959   Eq. (4). The diagonal line is the equality line $x = y$.

960

961   **Fig. 9.** Graph showing normalised cumulative deposition thickness Zn against cumulative

962   average slope θ_n for all the debris flows in this study. The curves used in each of the models

963   are 1 – exponential fit to debris flow 2DF, 2 – linear interpolation of data from flow 5DF, 3 –

964   sigmoidal curve fitted to flow 1DF to delineate the upper limit of the envelope of curves, and

965   4 – sigmoidal curve following the lower limit of the envelope of curves, derived by

966   translating curve 3 along the x-axis. See section 4.1 and appendix B for details.

967

968   **Fig. 10.** Graphic displaying the air photo mosaic of Ísafjörður taken by NERC ARSF overlain

969   with model debris flow paths derived from different curves fitted to the normalised

970   cumulative deposition thickness against cumulative average slope plot (Fig. 9), using starting

971   values given in Table 6, column 1. Arrows in upper left refer to tracks in Table 6.

972

973 **Table 1**

974 Dates of activity of the debris flows and dates of surveys described in this study[a]

975

Date	June 1999	June 2006	spring 2007	summer 2007	spring 2008	summer 2008
Event	2DF (1) 3DF (4) 4DF (5)	1DF	5DF	LiDAR and GPS survey	7DF (2DF*) 8DF 10DF	GPS Survey

976 [a]See Fig. 2 for geographical locations of numbered debris flows. Numbers in brackets
977 indicate the debris flow identification number in Decaulne et al. (2005) and * indicates debris
978 flow occurred along the same track as the debris flow in the brackets.

979 **Table 2**
980 Summary of estimated measurement and processing error generated during GPS data
981 collection and processing.
982

	Vertical Error (m)	Horizontal Error (m)
Human Error	0.05	0.05
GPS calculation error -wobble of antenna -constellation of satellites (number and position)	max = 0.121 mean = 0.01	max = 0.043 mean = 0.005
LiDAR	~ 0.25 (extremes up to 2 considering the horizontal error)	~ 1-2
LiDAR (post adjustment)	~0.1	< 0.25
Kriging Error 1DF	Variable, max = 0.85, mean = 0.11	Not calculated
Kriging Error 5DF	Variable, max = 0.42, mean = 0.07	Not calculated
Kriging Error – GPS only	max ~ 1.0 mean ~ 0.3	Not calculated
Kriging Error –LiDAR + GPS	max ~ 1.4 mean ~ 0.5	Not calculated
Kriging Error – from buffer	max ~ 1.6 mean ~ 0.9	Not calculated

983 **Table 3**
984 Summary of materials and drainage areas for each of the debris flows in this study.
985

Debris flow ID	Source material	Estimated clast-size range (estimated median) m	Estimated percent fines	angularity	Upstream area
1DF	Glacial deposits	0.01 - 4 (0.3)			
2DF	Glacial deposits	0.01 - 4 (0.3)	10-30	subrounded to subangular	Gleiðarhjalli bench
3DF	Glacial deposits	0.01 - 4 (0.3)			
4DF	Glacial deposits	0.01 - 4 (0.3)			
5DF	Talus and soil	0.01 - 0.2 (0.05)	30-50	mainly angular	Rock chute
7DF	Weathering of bedrock and reworked material	0.01 - 1.5 (0.2)		subangular to angular	Rock chute
8DF	Weathering of bedrock	0.01 - 0.8 (0.1)	< 5		
10DF	Weathering of bedrock	0.01 - 0.8 (0.1)			

986 **Table 4**

987 Summary of measured and estimated volumes and the other measured parameters of debris

988 flows in this study

989

Debris Flow ID	Measured deposition m^3 (Standard Error)	Measured erosion m^3 (Standard Error)	Estimated deposition m^3 (Standard Error)	Estimated erosion m^3 (Standard Error)	Elevation Drop (m)	Length (m)	Area (m^2)	Mean Width (m)
1DF			8000 (±66%)	41 000 (±38%)	391	756	20 087	26
2DF			2000 (±134%)	16 000 (±62%)	322	732	13 323	19
3DF			1000 (±124%)	6000 (±100%)	396	728	9327	13
5DF			100 (±136%)	400 (±81%)	88	198	1427	7
7DF*	800 (±105%)	600 (±160%)	500 (±76%)	2000 (±70%)	394	721	3858	9
8DF*	1000 (±94%)	200 (±195%)	700 (±100%)	700 (±123%)	571	797	3192	7
10DF*	1000 (±91%)	500 (±105%)	800 (±88%)	2000 (±60%)	590	866	4029	10

990 * indicates that the calculations performed do not include the debris flow source areas.

991 **Table 5**

992 Comparison of the results of Decaulne et al. (2005) with those from this study[a]

993

Debris Flow ID	Decaulne et al. (2005) estimated deposition (m^3)	Deposition (m^3) – this study	Deposition from linear lower surface (m^3) - this study	Deposition extrapolated from all cross sections (m^3) - this study	Deposition extrapolated from 3 cross sections (m^3) - this study
1DF	-	8287 (±66%)	11 584	7977	8359
2DF (1)	3000	1925 (±134%)	-	1770	2804
3DF (4)	1000	1119 (±124%)	-	-	-
5DF	-	136 (±136%)	128	-	-
7DF	-	562 (±160%)	531	-	-
8DF	-	211 (±195%)	918	-	-
10DF	-	495 (±105%)	806	-	-

994 [a]Numbers in brackets in the first column indicate the debris flow identification number in

995 Decaulne et al. (2005).

996 **Table 6**
997 Model results for three example flows, marked on Fig. 10, showing depth of the simulated
998 flow on reaching buildings for various starting volumes and planimetric areas[a]
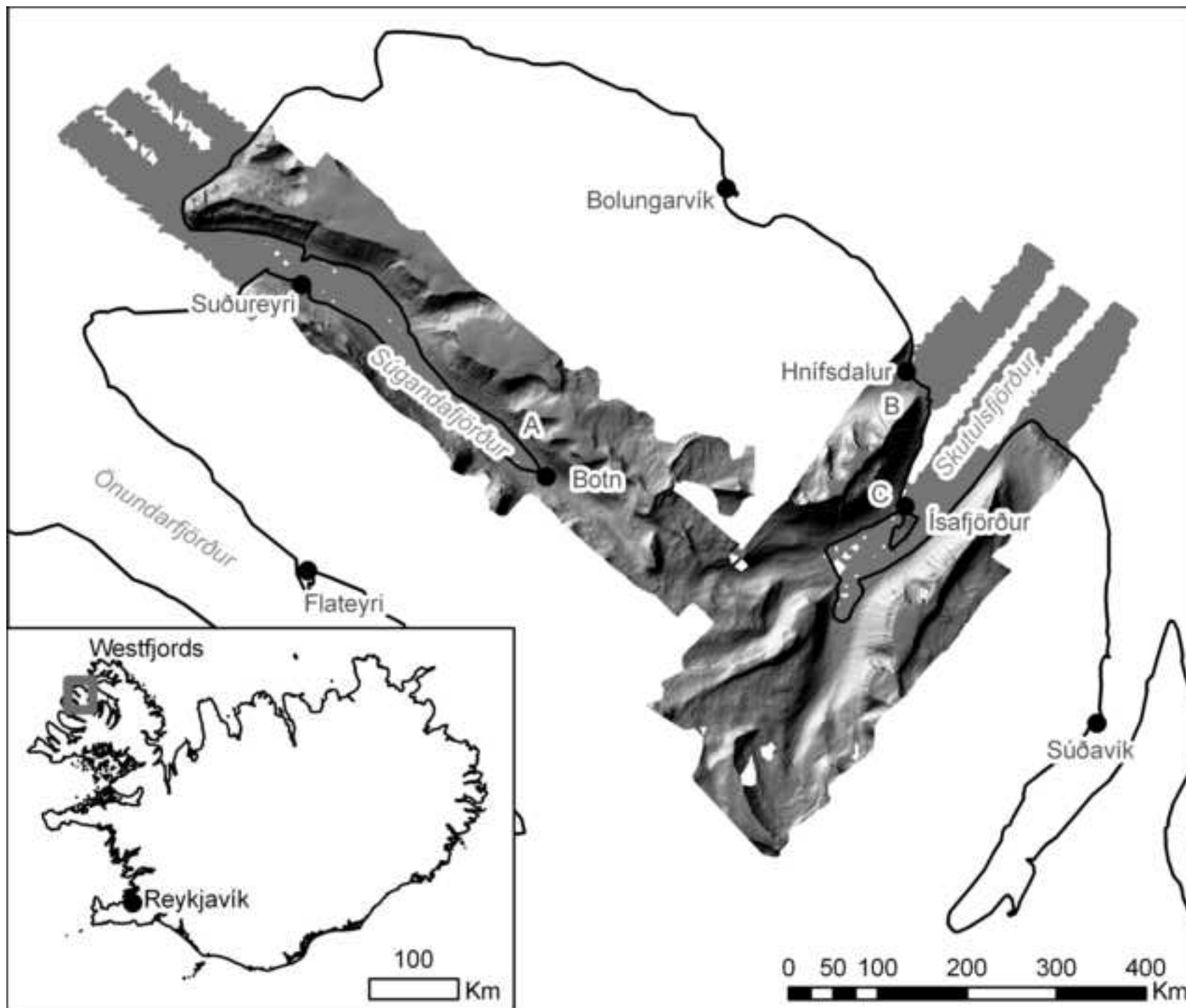999

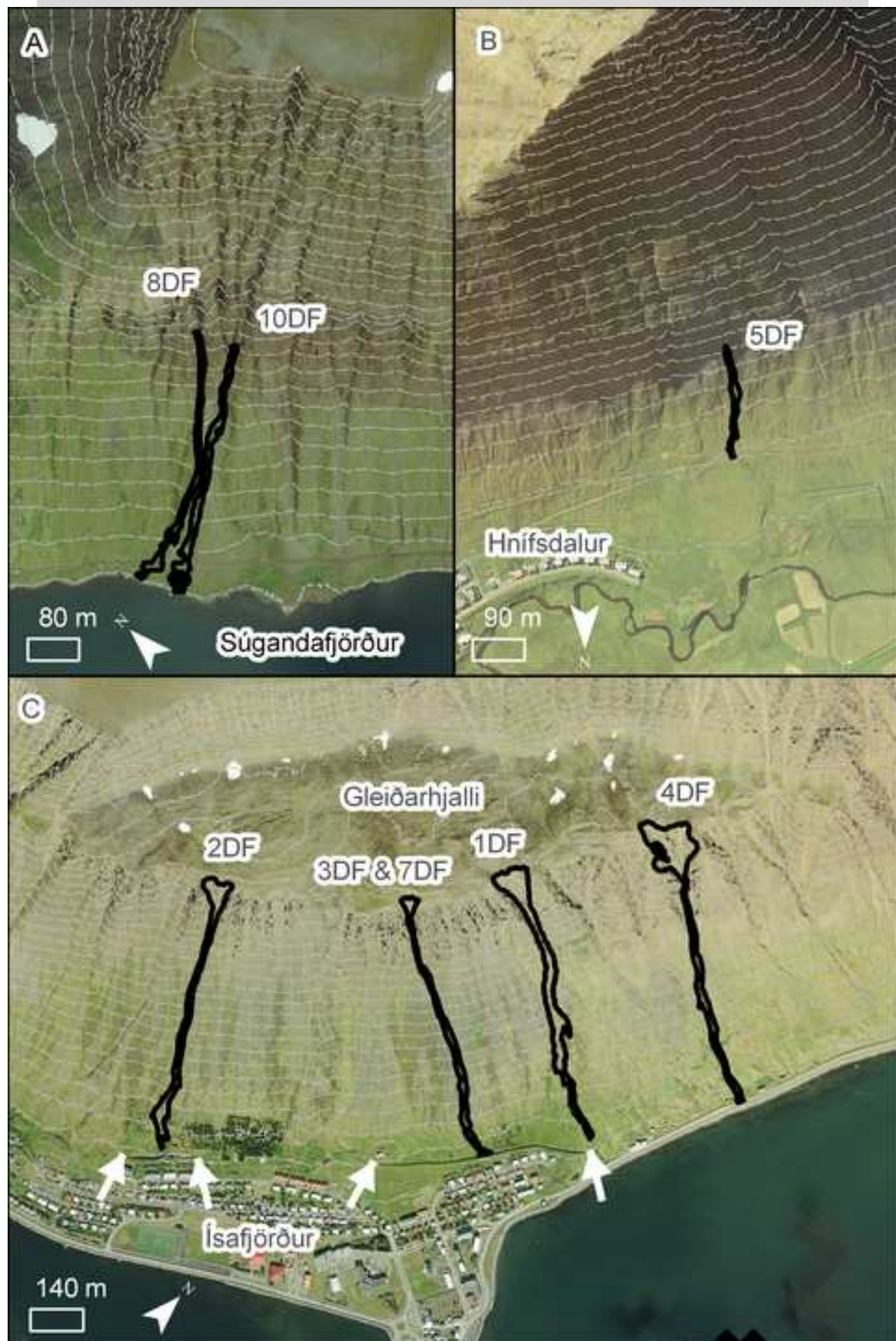| Starting volume (m³) : area (m²)		8 287 : 16 000	15 000 : 30 000	20 000 : 30 000
flow 1	**model 1 (m)**	0	0	0
	model 2 (m)	1.22*	1.22*	1.5*
	model 3 (m)	0	0	0
	model 4 (m)	1.16*	1.16*	1.6*
flow 2	**model 1 (m)**	0	0	0
	model 2 (m)	0.96	0.96	1.28*
	model 3 (m)	0	0	0
	model 4 (m)	0.73	0.73	0.97
flow 3	**model 1 (m)**	0	0	0
	model 2 (m)	0.99	0.99	1.32*
	model 3 (m)	0	0	0
	model 4 (m)	0.12	0.12	0.16

1000 [a]The first data column shows results from using the volume and area for debris flow 1DF in
1001 the models. Starred entries indicate where the thickness of the flows is > 1 m.

1002 **Table 7**
1003 Parameter values derived from least squares fits of functions given by Eqs. B5-B7 with their
1004 associated errors
1005

Equation	Parameter	Value	Error
B5	A	0.03267	0.01601
B5	B	1.87617×10^6	1.54541×10^6
B5	C	2.21702	0.1269
B6	A	35.04498	0.17543
B6	B	-8.52036	0.3586
B7	A	0.9834	0.00339
B7	B	-0.03816	0.00453
B7	C	36.30119	0.01725
B7	D	1.00308	0.01641

Figure 1

Figure 2

A
8DF
10DF
80 m
Súgandafjörður

B
5DF
Hnífsdalur
90 m
N

C
Gleiðarhjalli
4DF
2DF
1DF
3DF & 7DF
Ísafjörður
140 m

Figure 3

Erosion

Deposition

Underlying
DEM

5m

Figure 4

A   A'   B   B'   C   C'

50 m

Volume change (m):   -4 to 0   0 to 2.5
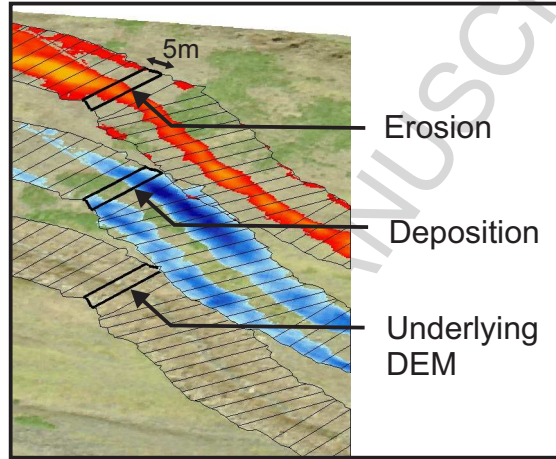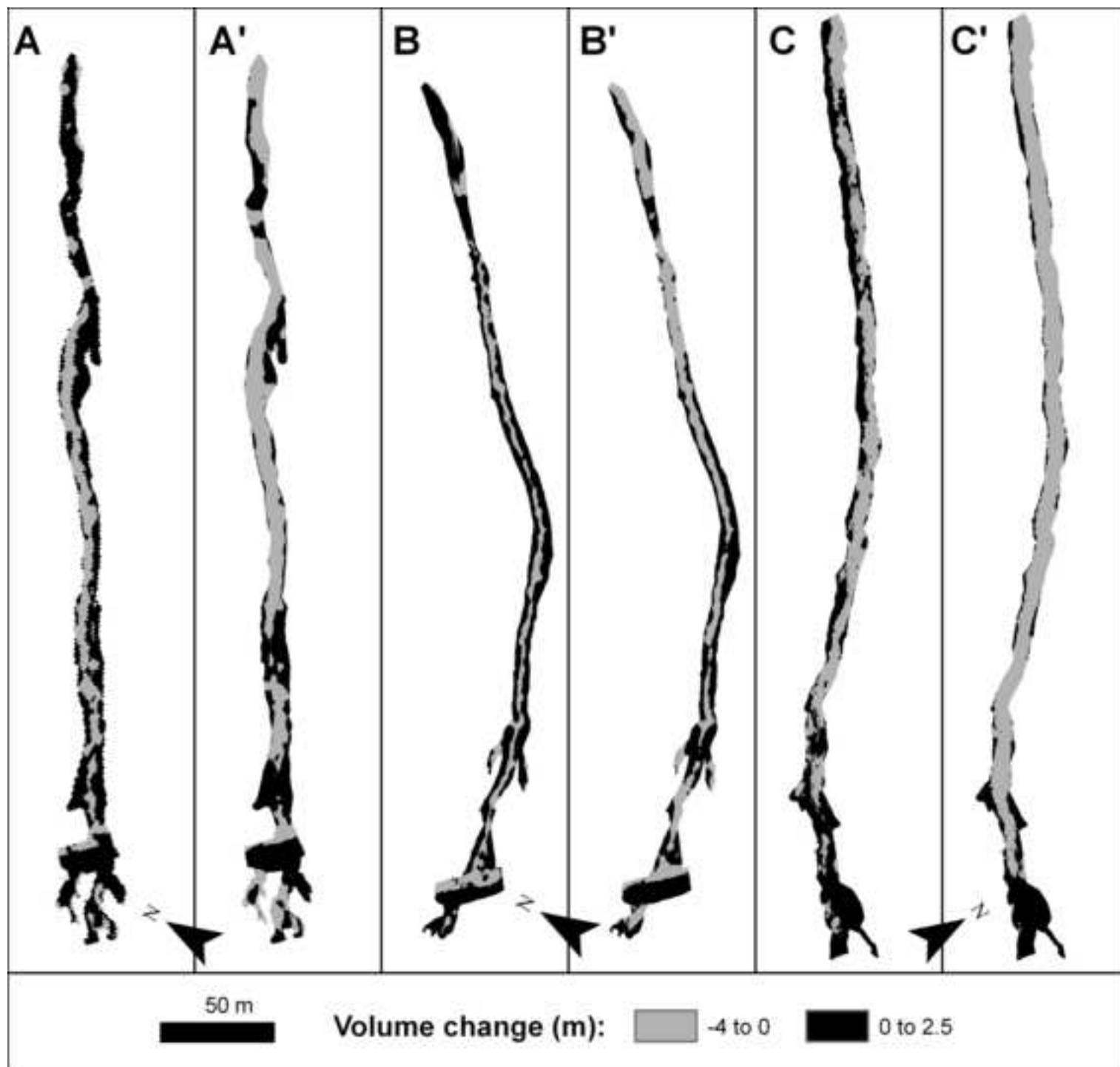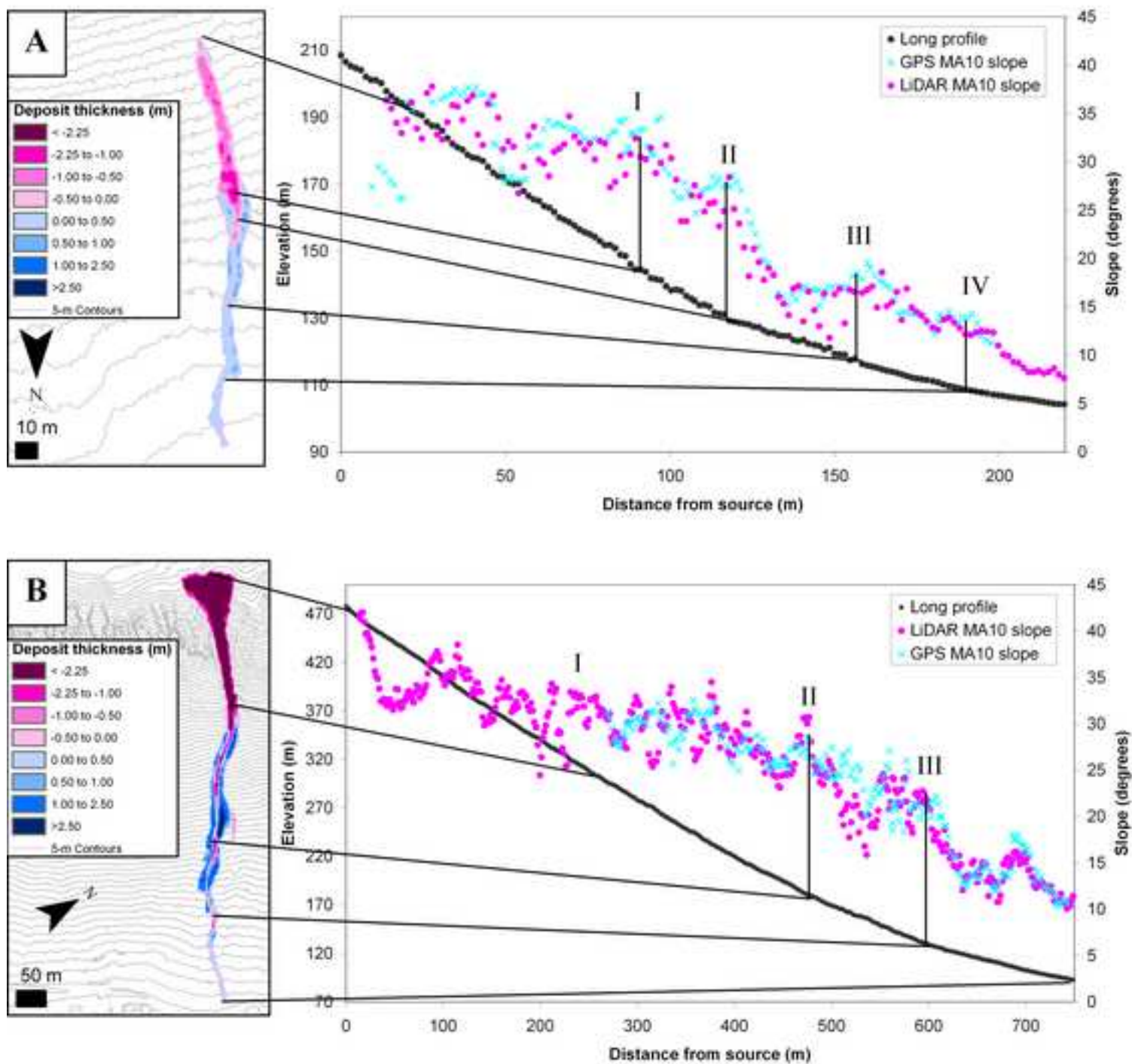
Figure 5

Figure 6

Figure 7

Figure 8

Figure 9

Figure 10

deposition
depth (m)

- none
- 0.00 - 0.10
- 0.10 - 0.25
- 0.25 - 0.50
- 0.50 - 0.75
- 0.75 - 1.00
- 1.00 - 1.50
- > 1.50

150 m

Model1

Model2

Model3

Model4